Detailed structures of the subducted Philippine Sea plate beneath northeast Taiwan: A new type of double seismic zone

Honn Kao and Ruey-Juin Rau

Institute of Earth Sciences, Academia Sinica, Taipei, Taiwan

Abstract. We studied the detailed structure of the subducted Philippine Sea plate beneath northeast Taiwan where oblique subduction, regional collision, and back arc opening are all actively occurring. Simultaneous inversion for velocity structure and earthquake hypocenters are performed using the vast, high-quality data recorded by the Taiwan Seismic Network. We further supplement the inversion results with earthquake source parameters determined from inversion of teleseismic P and SH waveforms, a critical step to define the position of plate interface and the state of strain within the subducted slab. The most interesting feature is that relocated hypocenters tend to occur along a two-layered structure. The upper layer is located immediately below the plate interface and extends down to 70–80 km at a dip of 40°–50°. Below approximately 100 km, the dip increases dramatically to 70°–80°. The lower layer commences at 45–50 km and stays approximately parallel to the upper layer with a separation of 15±5 km in between down to 70–80 km. Below that the separation decreases and the two layers seem to gradually merge into one Wadati-Benioff Zone. We propose to term the classic double seismic zones observed beneath Japan and Kuril as "type I" and that we observed as "type II," respectively. A global survey indicates that type II double seismic zones are also observed in New Zealand near the southernmost North Island, Cascadia, just north of the Mendocino triple junction, and the Cook Inlet area of Alaska. All of them are located near the termini of subducted slabs in a tectonic setting of oblique subduction. We interpret the seismogenesis of type II double seismic zones as reflecting the lateral compressive stress between the subducted plate and the adjacent lithosphere (originating from oblique subduction) and the downdip extension (from slab pulling force). The upper seismic layer represents seismicity occurring in the upper crust of a subducted plate and/or along the plate interface, whereas the lower layer is associated with events in the uppermost mantle.

1. Introduction

Northeast Taiwan is a tectonically complicated region (Figure 1). The Philippine Sea plate subducts beneath the Eurasia plate along the Ryukyu arc at a rate of 7±4 cm yr^{-1} [*Seno et al.*, 1993]. Most of the Ryukyu trench strikes NE–SW except to the west of 125°E where the orientation becomes nearly E–W. Bathymetric signature of the trench disappears to the west of 123°E. The western terminus of the arc is bounded by the active collision between the Luzon arc and Eurasia continent in the Taiwan region (Figure 1), an ongoing event that began ~4 Ma [e.g., *Lee and Lawver*, 1994; *Teng*, 1990; *Wu*, 1978b].

Previous studies have shown that seismic patterns along the Ryukyu arc vary systematically from north to south [e.g., *Kao and Chen*, 1991; *Shiono et al.*, 1980]. In addition to the typical subduction, the subducted Philippine Sea plate exhibits increasing amounts of lateral compression as it approaches Taiwan. Such a pattern is interpreted as a result of the transmitted strain originated from the collision [e.g., *Kao and Chen*, 1991; *Kao et al.*, 1998a]. Local seismicity clearly indicates that the subducted Philippine Sea plate extends west-

ward beneath NE Taiwan to a depth of at least 150 km (Plate 1) [e.g., *Kao et al.*, 1998a].

The regional tectonic setting is further complicated by the existence of numerous extensional features in the back arc region, namely, the Okinawa trough (Figure 1). Evidences from seismicity [e.g., *Ouchi and Kawakami*, 1989; *Sato et al.*, 1994], earthquake focal mechanisms [e.g., *Kao and Chen*, 1991; *Shiono et al.*, 1980], and seismic reflection profiles [e.g., *Sibuet et al.*, 1987] all indicate that the trough is actively deforming, presumably reflecting the present-day process of back arc opening.

Given the complex tectonic setting in the region, the purpose of this study is therefore to address the fundamental issue as how the subducted lithosphere responds to various tectonic processes, both compressional and extensional, at shallower depths. In particular, does the regional collision, which results in the complex orogeny in Taiwan, also have profound effects at depth? If indeed they do, what is the depth range and how are they reflected in terms of the seismogenic behavior within the subducted lithosphere?

To answer the above questions, we investigate the detailed configuration of the subducted Philippine Sea plate beneath NE Taiwan where subduction, collision, and back arc opening are all actively occurring. Our result is based on the joint inversion of three-dimensional (3-D) velocity tomography and relocation of earthquake hypocenters using the vast, high-quality data recorded by the Taiwan Seismic Network (Figure
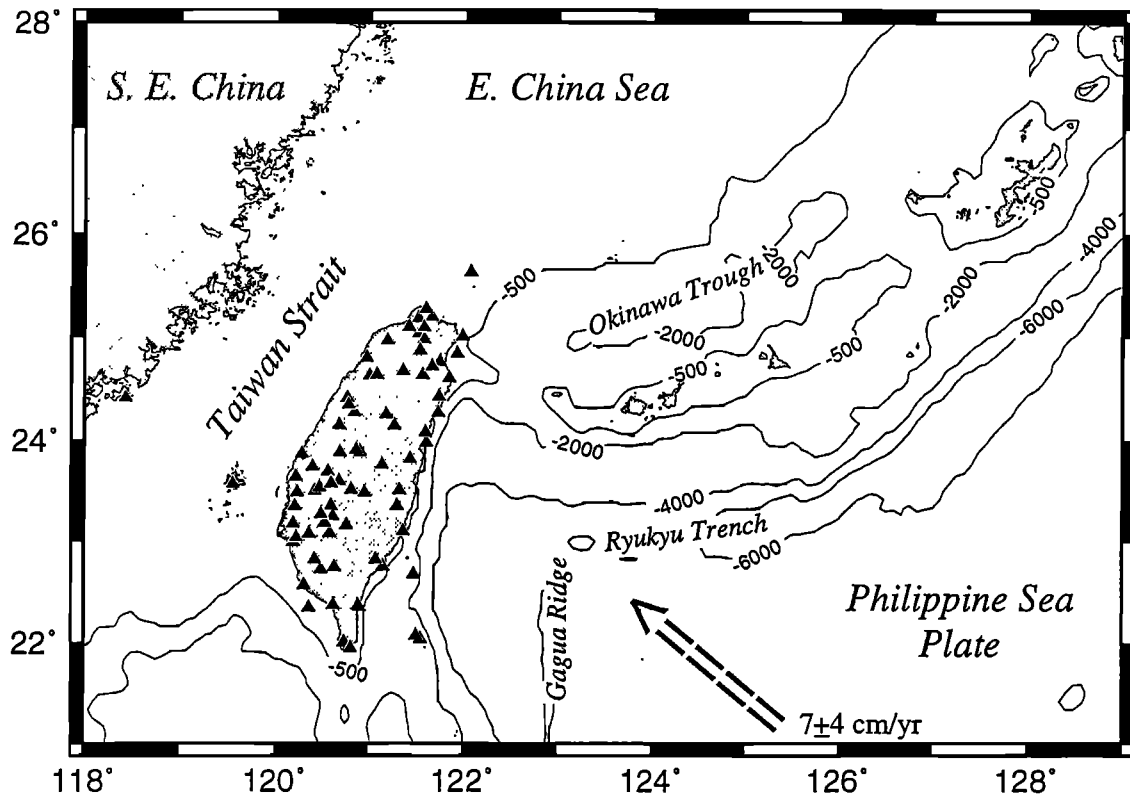
Figure 1. Map showing bathymetry in the Ryukyu arc–Taiwan region. Morphology of the Ryukyu trench disappears to the west of 123°E where it is intercepted by the Gagua Ridge. The Philippine Sea plate is moving at 7±4 cm yr^{-1} toward NW relative to the Eurasia plate, resulting in the Taiwan Collision Zone. The region is further complicated by the opening process of the Okinawa trough to the north. Solid triangles mark the station locations of the Taiwan Seismic Network. Its aperture and high-quality digital data provide excellent resolution to delineate detailed velocity structures associated with the subducted Philippine Sea plate underneath NE Taiwan.

1 and Plate 1) [*Shin*, 1993]. We further supplement the result with earthquake focal mechanisms and depths determined from inversion of teleseismic *P* and *SH* waveforms. This step provides critical information on the nature of distinct seismogenic structures and hence avoids the possibility of mistaking the interplate thrust zone or structures in the overriding plate as the Wadati-Benioff Zone (WBZ) [e.g., *Kao and Chen*, 1991, 1995; *Seno and Kroeger*, 1983].

In the following text we first examine the local seismicity along two profiles, one directly beneath NE Taiwan and another in the near offshore, to identify the overall configuration of the subducted Philippine Sea plate. The effects of regional collision are identified from the changing patterns of earthquake focal mechanisms. Then we show the results of joint inversion of 3-D velocity tomography and earthquake relocation. The most interesting feature of our results is that relocated hypocenters tend to form a two-layered structure (a double seismic zone). It differs from the classic double seismic zones (e.g., those observed beneath the Japan and Kuril arcs) in both geometry and depth range. To avoid any confusion, we propose to term the classic double seismic zones as "type I" and that we observed as "type II," respectively. We also find that the dip of WBZ steepens at depths greater than ~90 km.

Finally, we compare our results to similar studies in other major subduction zones and discuss the corresponding tectonic implications. It is noted that type II double seismic zones were documented previously along three regions: New

Zealand near the southernmost North Island [e.g., *Reyners et al.*, 1997], Cascadia just north of the Mendocino triple junction [e.g., *Smith and Knapp*, 1993], and Alaska in the Cook Inlet area [e.g., *Ratchkovsky et al.*, 1997]. All four regions have a common tectonic setting, that is, located near the terminus of an oblique subduction system with a significant lateral compressive stress field. We interpret the observed two layers of a type II double seismic zone as earthquakes in the subducted (and probably thickened) crust and uppermost mantle, respectively. The regional collision and subduction provide the necessary deviatoric stresses for the seismogenesis in the corresponding layers. Such an interpretation can also explain the large geometric variation of WBZ at depth.

2. Local Seismicity and Focal Mechanisms

Plate 1 shows the distribution of seismicity between 1991 and 1996 reported by the Seismological Observation Center of the Central Weather Bureau, Taiwan, along with the locations of local seismographic stations. While shallow seismicity is very intense along the eastern coastline and offshore, most earthquakes deeper than ~60 km occurred within the WBZ striking ~E–W that extends westward beneath NE Taiwan. The western boundary of the subducted Philippine Sea slab roughly follows the 121.6°E meridian between depths of 60 and 200 km. Earthquakes deeper than 200 km occurred mostly to the east of 122°E in a significantly less number.
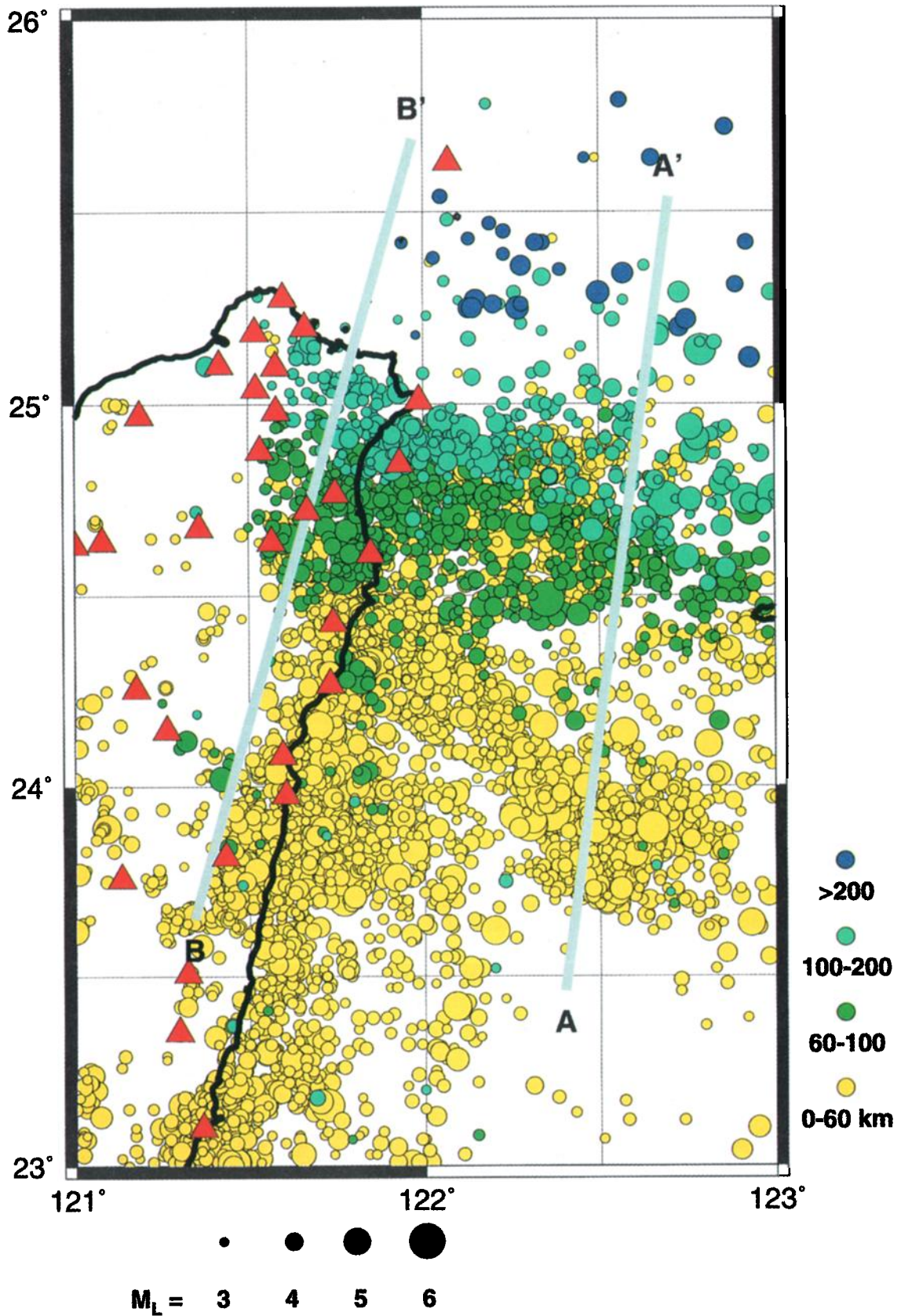
Plate 1. Map showing local seismicity in the southernmost Ryukyu arc–Taiwan region. Hypocenters (circles) were reported by the Seismological Observation Center of the Central Weather Bureau, Taiwan. Different colors and sizes represent different depths and magnitudes (M_L), respectively. Triangles show the station locations of the Taiwan Seismic Network. Profiles A–A' and B–B' mark the locations of cross sections in Figure 3 showing the distribution of projected hypocenters with depth.

Table 1. Source Parameters of Large- and Moderate-sized Earthquakes That Occurred in the Studied Region

Event[a]	Date	Origin Times[b], UT	Latitude[b], °N	Longitude[b], °E	Depth[c], km	Strike, deg.	Dip, deg.	Rake, deg.	m_b[b]	Seismic Moment, x10^17 N m	Reference[d]	Remark[e]
1	March 12, 1966	1631:19.9	24.24	122.67	22	36	73	165	6.6	4860	PW89	LC
2	May 5, 1966	1421:22.3	24.33	122.50	40	129	70	24	5.6	-	T83	LC
3	May 28, 1966	0003:59.2	24.29	122.55	44(0.5)±5	46±5	62±6	139±7	5.5	6.30±0.49	K98	LC
4	July 1, 1966	0550:38.0	24.86	122.56	110(0.5)±4	135±8	62±4	90±8	6.1	46.4±5.37	K98	DE
5	Oct. 25, 1967	0059:23.3	24.43	122.25	58(2.0)±5	37±3	37±3	132±5	6.0	205±44	K98	LC
6	Jan. 13, 1968	0703:45.8	24.13	122.21	27(3.3)±4	71±4	73±3	76±7	5.7	17.2±1.8	K98	LT
7	Nov. 27, 1970	0939:24.1	24.26	122.42	49(1.5)±6	11±13	42±10	115±14	5.7	3.94±0.80	K98	LC
8	Oct. 9, 1971	1315:38.5	24.86	122.03	95±8	175±8	73±6	68±10	5.7	3.72±0.42	K98	DE
9	April 24, 1972	0957:21.2	23.60	121.55	17(4.0)±4	36±11	41±4	132±6	6.1	164±23	K98	CT
10	March 14, 1978	2032:16.9	24.00	122.55	15	63	82	81	5.5	6.7	D87b	LT
11	Sept. 2, 1978	0157:34.2	24.81	121.87	88	54	47	152	6.0	80	PW89	DE
12	Jan. 29, 1981	0451:37.4	24.49	121.88	15	183	88	-128	5.7	10	D88	LC
13	Dec. 17, 1982	0243:03.8	24.56	122.53	80(2.0)±7	29±10	33±6	128±8	5.9	4.40±0.9	K98	DE
14	April 26, 1983	1526:40.2	24.67	122.63	115(2.0)±5	101±4	78±4	95±7	5.7	6.03±0.34	K98	DE
15	Sept. 21, 1983	1920:44.4	24.08	122.16	21(3.0)±5	78±6	71±3	71±12	6.0	28.9±3.3	K98	LT
16	Feb. 13, 1984	0448:57.7	25.47	122.38	269(4.0)±9	104±16	69±9	-75±17	5.5	2.35±1.50	K98	DC
17	Jan. 13, 1985	2151:22.5	24.12	122.48	36	156	66	57	5.8	1.73	D85	LC
18	Feb. 27, 1986	0623:13.3	24.02	122.23	15	69	77	80	5.8	5.7	D87a	LT
19	Feb. 12, 1988	1915:35.4	23.85	122.48	21(4.0)±11	76±8	82±8	81±17	5.6	1.40±0.32	K98	LT
20	Aug. 21, 1989	2312:41.4	24.09	122.48	19(3.0)±5	78±4	67±3	86±5	5.6	25.7±7.0	K98	LT
21	July 16, 1990	1914:51.7	24.25	121.82	9(1.0)±6	296±20	12±6	112±20	5.5	2.84±1.20	K98	LT
22	Dec. 13, 1990	0301:48.0	23.92	121.64	6(1.0)±4	12±11	87±4	92±16	5.9	57.0±16.0	K98	CT
23	Dec. 13, 1990	1950:17.9	23.72	121.63	10(1.0)±4	56±5	57±4	95±7	5.9	20.6±9.0	K98	CT
24	April 19, 1992	1832:00.2	23.86	121.59	14(0.5)±4	76±13	67±7	107±13	5.8	13.0±4.5	K98	CT
25	May 23, 1994	0536:01.6	24.17	122.54	32(3.0)±3	68±14	77±7	78±14	5.7	12.7±4.4	K98	LT
26	June 5, 1994	0109:30.1	24.51	121.90	8(1.0)±4	178±5	76±4	125±9	6.1	32.8±14.0	K98	CT
27	Feb. 23, 1995	0519:01.9	24.14	121.61	34±4	5±6	78±4	80±11	5.9	11.8±1.4	K98	CT
28	June 25, 1995	0659:06.2	24.60	121.70	47(1.0)±6	36±4	68±3	146±5	5.8	6.98±1.90	K98	LC

[a]Events are numbered in chronological order.
[b]Epicenters, origin times, and magnitudes are those reported in the Bulletin of the International Seismological Centre (ISC) and the Preliminary Determination of Epicenters (PDE) for events before and after 1988, respectively.
[c]Depth below sea level. Where applicable, the value inside parentheses is the thickness of the water column above the source region.
[d]T83, Tsai et al., 1983; PW89, Pezzopane and Wesnousky, 1989; K98, Kao et al., 1998a; D85, Dziewonski et al., 1985; D87a, Dziewonski et al., 1987a; D87b, Dziewonski et al., 1987b; D88, Dziewonski et al., 1988.
[e]LC, lateral compressional mechanism; LT, low-angle thrust mechanism; DE, downdip extensional mechanism; DC, downdip compressional mechanism; CT, collisional thrust mechanism.
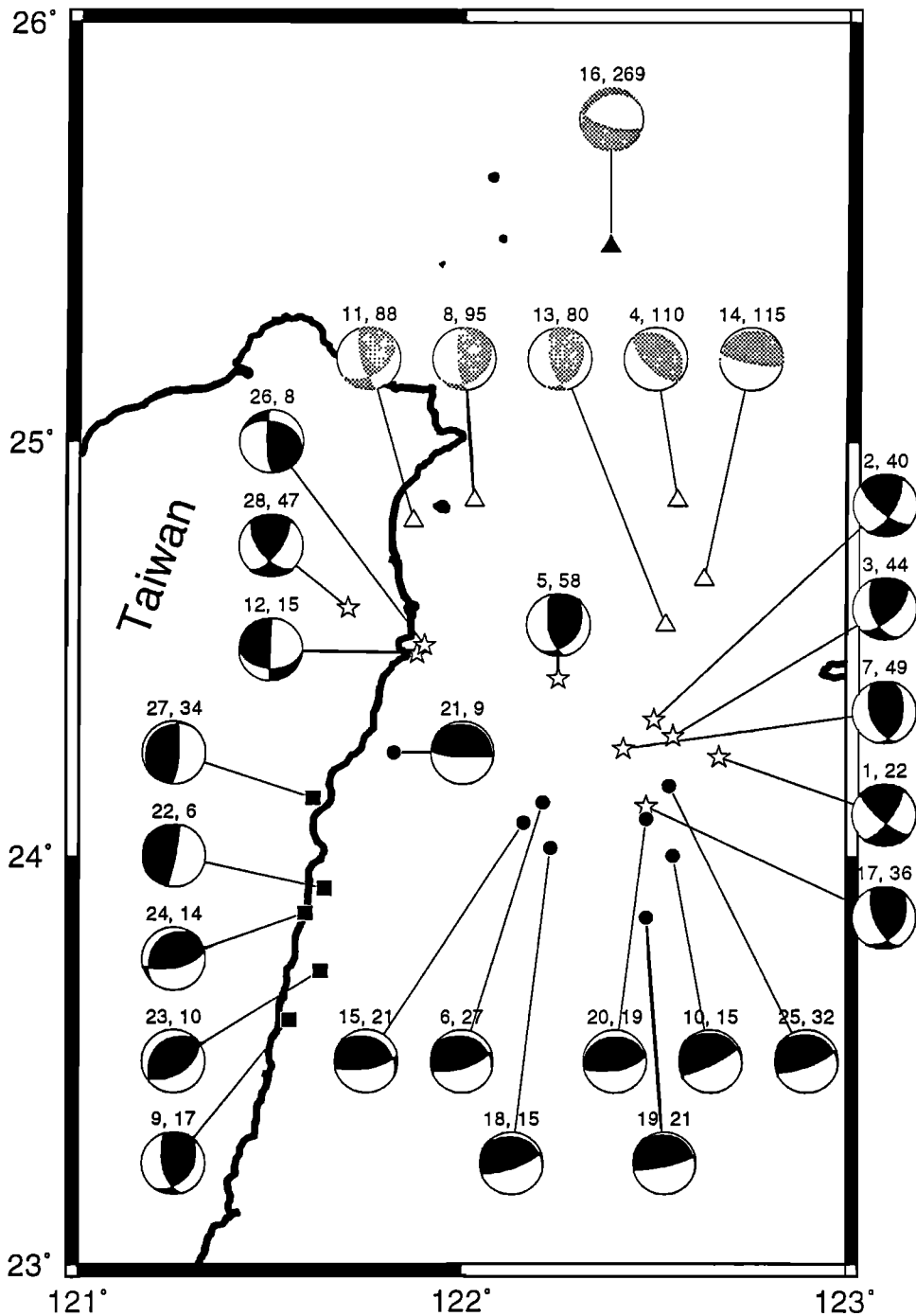
Figure 2. Map showing the epicenters and focal mechanisms of large- and moderate-sized earthquakes occurring in the region. Equal-area projections of the lower hemispheres of the focal spheres for 28 earthquakes selected from *Kao et al.* [1998a] are plotted showing the orientation of the nodal planes. Darkened areas show quadrants with compressional *P* wave first motions; black and gray shadings represent events shallower and deeper than 60 km, respectively. Each fault plane solution is labeled by the corresponding event number and focal depth (according to Table 1). Four major seismogenic structures associated with the subducted Philippine Sea plate are delineated, as indicated by different symbols for epicenters: collision seismic zone (solid squares), interface seismic zone (solid circles), Wadati-Benioff Zone in downdip extension (open triangles) and compression (solid triangle), and lateral compression seismic zone (open stars).

Kao et al. [1998a] recently determined the source parameters of large- and moderate-sized earthquakes that occurred in the region to investigate the characteristics of transition from the oblique subduction in the southernmost Ryukyu arc to the collision in Taiwan. Precise focal depths and mechanisms were determined from inversion of teleseismic *P* and *SH* waveforms [*Nábelek*, 1984]. We adapt their results and listed 28 selected earthquakes in Table 1. In Figure 2, these events are separated into groups, as represented by different symbols, based on their distinct characteristics of focal mechanisms.
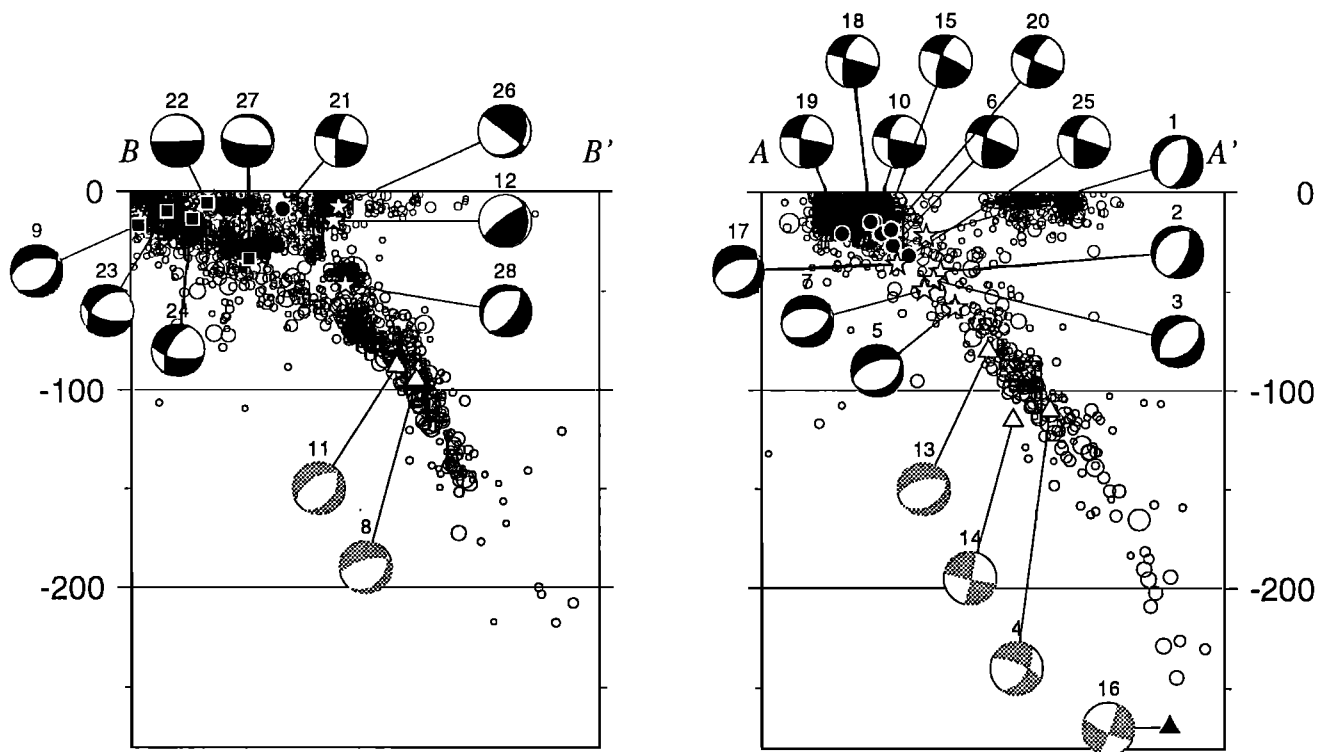
Figure 3. Cross sections (without vertical exaggeration) showing local seismicity and focal mechanisms along profiles A–A' and B–B' in Plate 1. Fault plane solutions of earthquakes in Table 1 and Figure 2 (within ~50 km from the profiles) are shown in equal-area projection of the back hemisphere of the focal sphere. Layout of shadings and small symbols are the same as in Figure 2. In cross section A–A', a typical subduction zone is observed, with the addition of earthquakes showing lateral compressional strain (events 1, 2, 3, 5, 7, and 17). The seismogenic portion of plate interface is clearly shown by many low-angle thrust earthquakes at shallow depths. The Wadati-Benioff Zone (WBZ) dips at 40°–50° between 60 and 130 km, but steepens slightly to ~60° at greater depths. The seismic patterns in cross section B–B', on the other hand, show two major features. Earthquakes at shallow depths are mostly thrust events related to the regional collision. Only one low-angle thrust event (21) is observed that marks the position of plate interface to the east of this profile. The intraplate seismicity within the subducted plate seems to distribute along a two-layered structure that spans from ~40 to ~80 km.

At shallow depths (≤35 km), the predominant feature is the large number of events showing low-angle thrust mechanisms located to the east of Taiwan (events 6, 10, 15, 18, 19, 20, 21, 25; solid circles). These events presumably reflect the relative slip between the subducted Philippine Sea plate and the overriding Eurasia plate along the interface. The collision-related compressive strain is represented by two groups: one along the eastern coastline at depths less than 35 km (collision seismic zone; events 9, 22, 23, 24, 27; solid squares) and another extending eastward from NE Taiwan to southern Ryukyu in a wider deep range (lateral compression seismic zone; events 1, 2, 3, 5, 7, 12, 17, 26, 28; stars). All these events have maximum compressive axes (P axes) in either E–W or NE–SW directions. Earthquakes in the shallow part of WBZ (≤120 km; events 4, 8, 11, 13, 14; open triangles) consistently show maximum tensile axes (T axes) in the slab's downdip direction (i.e., downdip extension). However, the state of strain switches to downdip compression at a greater depth, as indicated by event 16 (solid triangle; Figure 2).

In Figure 3, local seismicity (Plate 1) and focal mechanisms (Figure 2) are plotted together along two profiles trending N15°E–S15°W, a direction approximately perpendicular to the strike of the subducted slab. Along the eastern

profile A–A', the configuration of seismogenic structures is basically the same as that in the southern Ryukyu arc [e.g., Kao and Chen, 1991]. While intense seismicity was found along the plate interface and in the back arc region, lateral compressional earthquakes were observed at some greater depths (≤50 km). The WBZ has an average dip of 40°–50°, as clearly defined by numerous intraplate earthquakes occurred between 60 and 130 km. Below that, it seems to steepen slightly to ~60°, although the number of events is significantly less.

On the other hand, seismic patterns along profile B–B' show two major features. For depths >40 km, the subducted Philippine Sea plate extends westward to beneath this profile and is clearly visible. The plate boundary at shallow depth, however, is greatly distorted and located to the east of this profile [Kao et al., 1998a], as represented by event 21 showing typical low-angle thrust mechanism (Table 1 and Figure 2). The densely distributed earthquakes at depths <40 km show predominating thrust faulting with P-axes in E–W/NE–SW directions (Figures 2 and 3). They presumably reflect the ongoing process of collision and may not be associated with the subduction of Philippine Sea plate at all. Setting aside the collision-related events at shallow depths, intraplate seis-

micity within the subducted lithosphere seems to distribute along a two-layered structure that spans from ~40 to ~80 km. At a first glance, this could be an artifact from depth uncertainty. However, as we shall illustrate in the next section, the two-layered distribution of seismicity becomes even better defined after the joint inversion of 3-D velocity tomography and earthquake relocation. The average dip of the WBZ seems to increase with depth from ~35° at 40 km to ~65° at ≥100 km.

It is interesting to note that events showing P axes parallel to the local strike of the arc are all confined at depths less than ~100 km (Figure 3). These lateral compressional events also show consistent T axes in the downdip direction of the subducted slab if they occurred between 40 and 100 km, presumably within the WBZ (e.g., events 1, 2, 3, 5, 7, 13, 17 in profile A–A' and events 8, 11, 28 in profile B–B'; Figure 3). Such a pattern can be explained as the result of interaction between the compressive stress regime due to regional collision (which is most significant within the lithosphere in the lateral direction [Kao and Chen, 1991]) and the downdip extensional stress regime due to slab subduction [e.g., Spence, 1987]. Furthermore, there seems to have no obvious difference between the focal mechanisms of events in the upper (events 1 and 28) and lower (events 2, 3, 5, 7, 8, 11, 13, and 17) layers.

3. Three-Dimensional Tomography and Relocation of Earthquake Hypocenters

With the help of focal mechanisms of large and moderate-sized earthquakes, it is rather straightforward to identify the state of strain of various seismogenic structures. Nonetheless, the locations of hypocenters reported in local bulletins might lack the required resolution to constrain the detailed geometry of the subducted slab because possible mislocation resulted from assuming a 1-D layered model could introduce some artifacts to the image. Such examples have been suggested by many previous studies to explain an apparent kink of WBZ at ~100 km beneath the Alaska–Aleutian arc [e.g., Frohlich et al., 1982; Hauksson, 1985; McLaren and Frohlich, 1985].

Consequently, we perform a joint inversion for 3-D velocity tomography and earthquake relocation by taking advantage of the vast, high-quality digital data recorded by the Taiwan Seismic Network. Considering the distribution of seismic stations (and therefore the tomographic resolution of data; Plate 1), we focus our efforts on the NE Taiwan region that is completely covered by the network.

3.1. Data and Method

The Taiwan Seismic Network has a total of 75 stations distributing densely on Taiwan and offshore islets (Figure 1). Three-component, digital data (sampling at 100 Hz) are transmitted real time to the Seismological Observation Center of the Central Weather Bureau where the routine determination of earthquake hypocenters is performed. From January 1, 1991, to March 31, 1997, a total of 69,024 earthquakes ranging from 0.5 to 7.0 in M_L were reported. Out of this data set, 2480 events are selected for the inversion (Figure 4). The event selection criteria are (1) the earthquakes having P arrivals recorded at more than eight stations and (2) the largest azimuthal gap between stations being less than 180°. Seismograms recorded at 39 stations in the northern part of Taiwan are carefully examined to determine arrival times for the first P and S phases. To ensure the highest accuracy in time,

only prominent arrivals are admitted into our data set and only horizontal components are used to time S observations. In general, the reading error is limited to only a few sampling intervals (i.e., 0.02–0.05 s). The total numbers of P and S arrivals used in the inversion are 42,806 and 22,256, respectively.

We used a grid system of 10 layers with the orthogonal directions parallel (N15°E, the Y direction) and perpendicular (S75°E, the X direction) to the local strike of the slab (Plate 1 and Figure 4). The dimension of our model is 100 km (X direction) by 110 km (Y direction) by 150 km (depth). The distance between each layer depends on the average number of passing rays, ranging from 5 km at the top to 40 km at the bottom. Seismic velocities and locations of hypocenters were inverted iteratively by a damped, linear, least squares technique from the observed arrival times, as depicted by Thurber [1983, 1993] and Evans et al. [1994].

The 3-D inversion converged after six iterations, reducing the weighted root-mean-square (RMS) arrival time residual from its initial value of 0.34 to 0.21 s. The average uncertainties of earthquake locations are 3 km horizontally and 5 km vertically. For some deeper earthquakes and those occurred just outside the network, uncertainties may increase to 10 km horizontally and 15 km vertically.

To quantify the goodness of fit of the model parameters, two approaches were employed in this study. First, the spread function of the model resolution was calculated based on the L_2 norm of the difference between the resolution matrix and an identity matrix [Menke, 1989]. Velocity grid point with smaller spread function represents higher resolution. Second, a synthetic test named "restoring resolution test" [Zhao et al., 1992] was conducted. The test takes the tomographic image obtained by inverting the real data set as the reference and computes the synthetic travel times between the source and receiver locations. After adding random noise, the same inversion procedure was performed using the synthetic data set. By comparing the two inversion results, we may know how well the tomographic features can be recovered.

3.2. Results

Plate 2a shows a cross section along profile C–C' in Figure 4. The location of this profile follows much of the profile B–B' in Plate 1, only being slightly shorter as limited by the dimension of the seismic network. Relocated hypocenters to the east of the profile within a distance range of 25 km are projected onto the cross section to best show the detailed geometry of WBZ.

The most interesting feature in Plate 2a is the significant difference in the seismic patterns within the subducted Philippine Sea plate at greater depths and in the collision zone at shallow depths. In the collision zone, earthquakes take place more or less uniformly between 0 and 50 km, whereas in the Philippine Sea plate earthquakes tend to occur along a two-layered structure and form an apparent double seismic zone. The location of the upper layer is immediately below the interplate thrust zone inferred from earthquake focal mechanisms (Figure 3). This layer extends down to 70–80 km at a more or less constant dip of 40°–50°. Below approximately 100 km, the dip increases dramatically to 70°–80°. In other words, there seems to have a significant geometric variation in the shape of the WBZ across the depth range of 70–100 km.
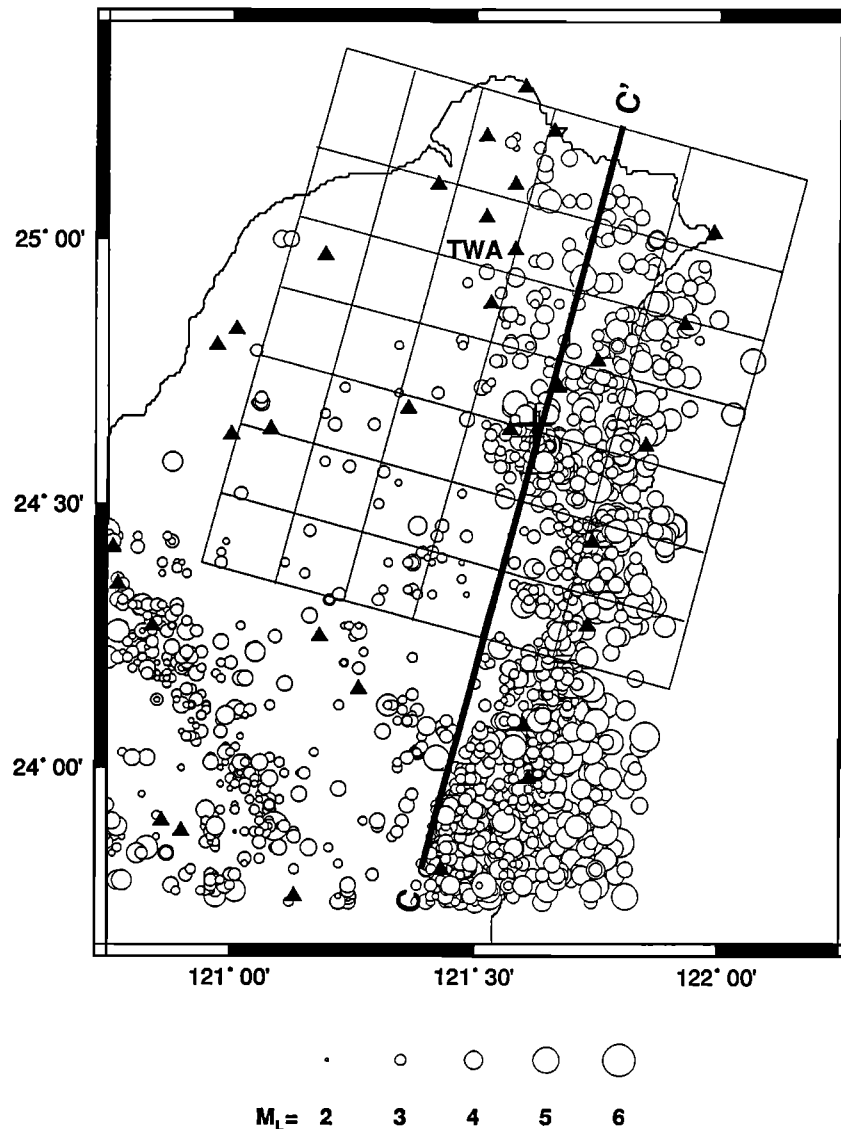
Figure 4. Distribution of earthquake epicenters (open circles) and stations (solid triangles) used in our joint inversion for velocity structure and hypocentral locations. The grid system consists of 10 layers with the orthogonal directions parallel and perpendicular to the local strike of the slab. Profile C–C' marks the location of cross section shown in Plate 2 and Figure 5. The plus marks the earthquake that generated clear S to P converted phase recorded at station TWA, as shown in Figure 6.

The lower layer commences at 45–50 km and maintains approximately parallel to the upper layer with a separation of 15±5 km in between down to 70–80 km. Similar to the upper layer, the dip of the lower layer increases at depths ≥90–100 km, but with a value of about 10°–15° less. Thus the distance between the two layers decreases with increasing depth and they seem to merge into one WBZ at depth ≥130 km.

The result of our 3-D relocation makes the gap between the two seismic layers more prominent (compare Plate 2a to the profile B–B' in Figure 3). In Figure 5a, we plot the corresponding hypocentral uncertainties. From the distribution of uncertainties, it seems very unlikely that the separation of the two layers is merely due to mislocation of earthquake hypocenters, particularly for depths between 40 and 80 km where the resolution of our 3-D tomographic inversion is good (a subject we shall address next). At 80 km and below, the gap

between the two layers is not well defined because the relocation errors of earthquakes occurred in the upper layer seem to overlap with that of the lower layer. This pattern implies that the two layers are separated by no more than ~15 km at greater depths.

The tomographic image clearly shows a high-velocity anomaly dipping toward north with increasing depth (see the 8.0 and 8.5 km s⁻¹ isopachs in Plate 2a), presumably indicating the location of the subducted slab. The location of this high-velocity anomaly is consistent with the distribution of seismicity. The 8.0 km s⁻¹ isopach follows approximately the top boundary of the upper seismic layer between depths of 50 and 90 km. In addition to the high-velocity anomaly observed at depth, a prominent low-velocity region is mapped directly above the subducted slab in the back arc region, which probably corresponds to the mantle wedge (Plate 2a). Previous
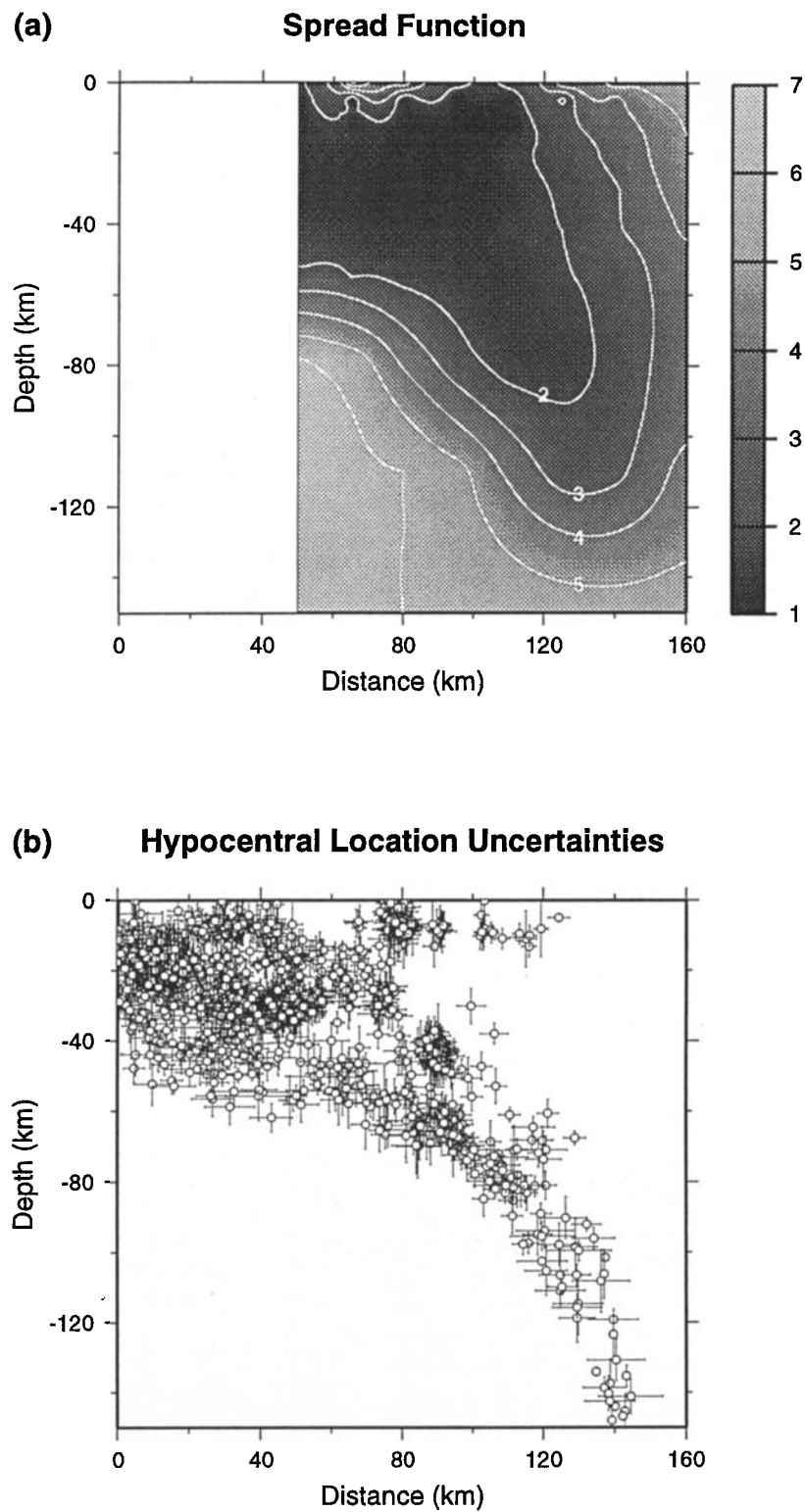
Figure 5. (a) The associated distribution of spread functions. Smaller number means higher resolution. Similar to Plate 2b, most tomographic images are well resolved (<3) except for regions near the northern and bottom edges of our model. (b) The hypocentral uncertainties of earthquakes. It seems very unlikely that the separation of the two layers is merely an artifact due to earthquake mislocation.

seismic and geodetic studies have suggested that the Ilan Plain is under strong influence of the Okinawa trough system [e.g., *Yeh et al.*, 1989; *Liu*, 1995]. Our results indicate that the center of the opening can be traced down to as deep as ~30 km, as shown by the 6.0 km s^{-1} isopach. Seismic activities inside the trough concentrate within the very top 10 km, a pattern consistent with the inference that the low-velocity anomaly is associated with the partial melting of crustal materials responsible for the Okinawa trough opening.

Plate 2b and Figure 5a show the result of "restored resolution test" and the spread function associated with our 3-D inversion. For the synthetic test, random noise in normal (Gaussian) distribution with standard deviations of 0.05 s (the largest possible reading error), 0.1 s, 0.2 s, 3 km, and 5 km was added to the error-free *P*, *S-P* arrival times, origin times, horizontal, and vertical hypocentral locations, respectively. Three inferences can be concluded from these results. First, the tomographic images obtained from the inversion of real data are, on the whole, correctly reconstructed from the synthetic data. Second, the resolution is generally good for the obtained images. All the important tomographic features (e.g., the subducted lithosphere and the Okinawa trough) have spread functions less than 3, indicating that they are not artifacts due to insufficient data resolution. Finally, although the resultant hypocenters from inversion of the synthetic data are more scattered than that from real data, main patterns of earthquake distribution remain unchanged.

Notice that the difference in calculated travel time using between the Cartesian coordinate (Thurber's code, this study) and the spherical coordinate (which should be used for the Earth being a sphere) may exceed 0.1 s if the epicentral distances and focal depths are greater than ~120 and 100 km, respectively [*Sato*, 1978]. Such a calculated travel time error (0.1 s) is slightly higher than the overall reading error of our data set and may affect the resolution of the resulted velocity images and/or the relocated hypocenters. Fortunately, less than 0.5% of our data are in the ray path range corresponding to greater travel time errors and all of them have focal depths >100 km, thus having little effect on the focus (depths < 80 km) of the present study.

3.3. Possible Hypocentral Mislocation

It is well documented in the literature that a high-velocity subducted slab might introduce significant hypocentral mislocation that leads to artifacts in the seismic pattern. One of the most famous examples is the sharp kink in WBZ along the central and eastern Aleutian at a depth of ~110 km [e.g., *Engdahl*, 1977; *House and Jacob*, 1982; *Reyners and Coles*, 1982]. While seismicity shows the WBZ in two segments with the deeper dips 20° more than the shallower one, many studies argued that the sharp dip increase is merely an artifact due to systematic mislocation of hypocenters using local data with conventional layered model [e.g., *Frohlich et al.*, 1982; *Hauksson*, 1985; *McLaren and Frohlich*, 1985].

Another source of mislocation is due to the poor azimuthal coverage and/or limited aperture of local networks. According to the control study of *McLaren and Frohlich* [1985], earthquake hypocenters located by a local network with most stations distributed along the strike of arc (i.e., on small volcanic islands) could be shifted by as much as 100 km. Furthermore, there would be an apparent increase in the dip of WBZ beneath a certain depth.

In our case, owing to the unique tectonic setting of arc-continent collision, the station distribution is excellent such that the local network has sufficient aperture in both along- and normal-to-the-arc directions (Figure 4). This advantage provides tight constraints on the earthquake hypocenters and thus significantly reduces the possible location error. As far as the slab effect is concerned, we have performed joint inversion of 3-D velocity tomography and earthquake relocation, a process that automatically takes various velocity anomalies into account, including not only the high velocity subducted Philippine Sea slab but also the low-velocity Okinawa trough at shallower depths. Hence we believe that the various effects of hypocentral mislocation on our results should be minimum.

Finally, it is noted that the mislocation resulted from either 3-D velocity complexity or inadequate network configuration is by no means random but systematically increasing with depth [e.g., *McLaren and Frohlich*, 1985]. Thus even if the slab effects cannot be completely eliminated, the most we would expect is a slight change in the dip angle of WBZ at depth. It seems unlikely to radically overthrow our inferences of the existence of a type II double seismic zone between 40 and 100 km and the significant geometric variation of the subducted Philippine Sea plate.

4. Interpretations and Discussion

From the location of low-angle thrust earthquakes and the high-velocity anomaly in the tomographic image (Figures 3 and 5 and Plate 2), it seems that the two-layered WBZ is located within the subducted Philippine Sea plate with the upper layer immediately below the top boundary of the slab. To further confirm this inference, which is crucial to possible interpretations, we carefully examine a large quantity of seismograms looking for converted phases to pinpoint the top boundary of the subducted lithosphere [e.g., *James and Snoke*, 1994; *Matsuzawa et al.*, 1986; *Zhao et al.*, 1997]. Our efforts had limited success, and one example is shown in Figure 6.

The event took place near the top of the lower seismic zone at 65 km and the recording station (TWA) is in northern Taiwan (Figures 4 and 6b). The particle motion of the prominent converted phase (marked by an "*X*" in Figure 6a) clearly resembles that of the *P* rather than *S* phases, suggesting that it is probably an *S*-to-*P* conversion at the top boundary of the subducted plate. The time differences from *P* to *X* and from *X* to *S* are 1.69 and 6.25 s, respectively. Given the 3-D velocity model (Plate 2 and Figure 5), they correspond to a boundary 17–20 km above the hypocenter (Figure 6b), a pattern remarkably consistent with our previous conclusion. Unfortunately, we were unable to find sufficient number of clear converted phases to map out the boundary of the subducted plate in further detail. Future deployment of a densely distributed high-resolution broadband array in the region would probably be necessary to resolve the issue.

4.1. Double Seismic Zones: Type II versus Type I

Double seismic zones within the subducted slab were documented for the Japan and Kuril arcs more than two decades ago [e.g., *Umino and Hasegawa*, 1975; *Veith*, 1974]. Subsequently, double seismic zones have been reported for several other regions, including various segments along the Japan arc [e.g., *Hasegawa et al.*, 1978; *Kawakatsu and Seno*, 1983; *Matsuzawa et al.*, 1986], the Kuril arc [e.g., *Kao and*
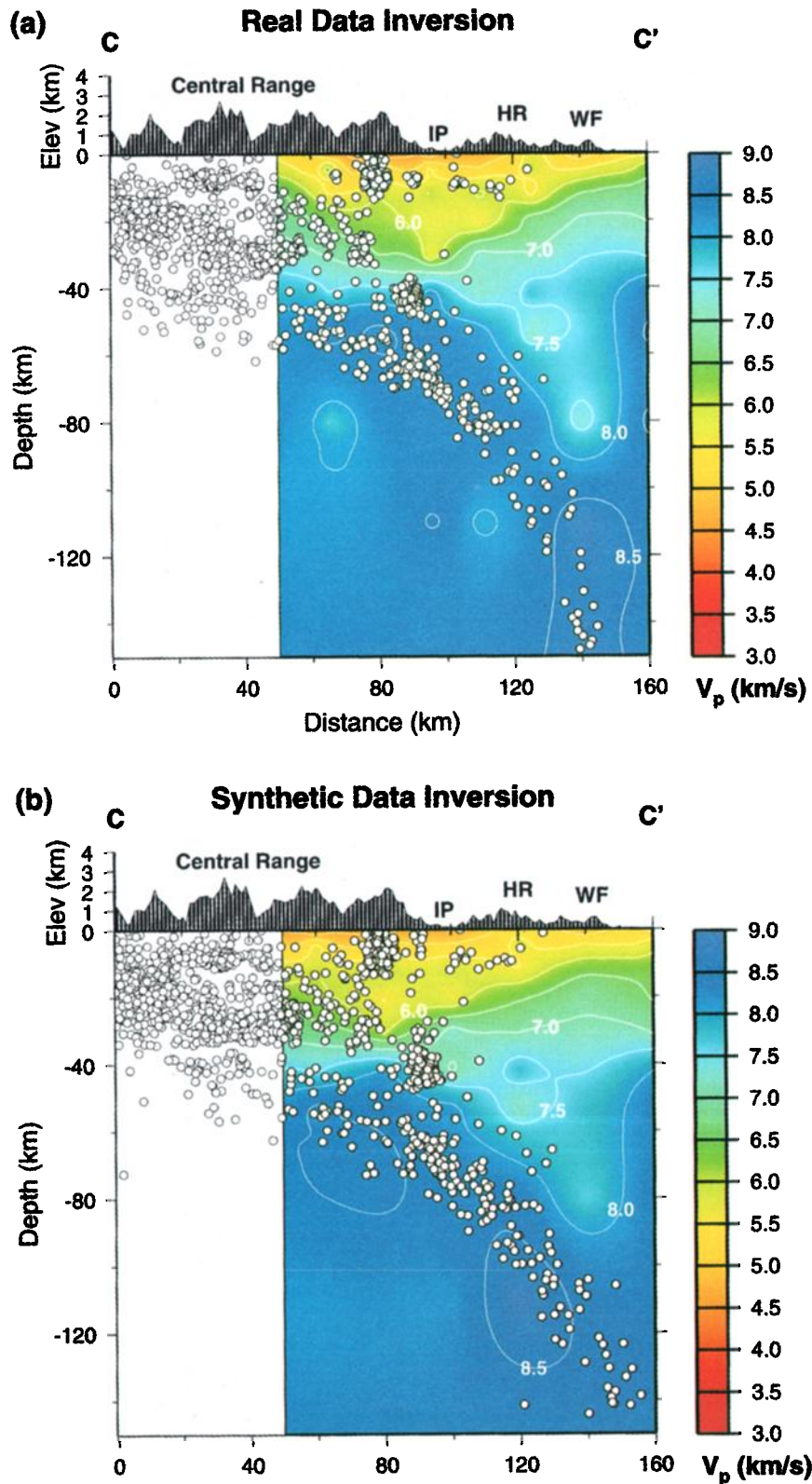
Plate 2. (a) Cross section showing the inversion results of tomography and earthquake relocation. Surface topography is at the top showing the locations of Western Foothills (WF), Hsuehshan Range (HR), and Ilan Plain (IP, which is the western extension of the Okinawa trough). The subducted Philippine Sea plate and Okinawa trough are clearly shown by high- and low-velocity anomalies at deep and shallow depths, respectively. Relocated hypocenters clearly distribute along a two-layered structure (a double seismic zone). The separation between the two layers is 15±5 km down to a depth of 70–80 km. Below that, the two layers seem to gradually merge into one Wadati-Benioff Zone. (b) Results of "restoring resolution test." Most of the tomographic images and seismic patterns on Plate 2a can be successfully reconstructed from the synthetic data.
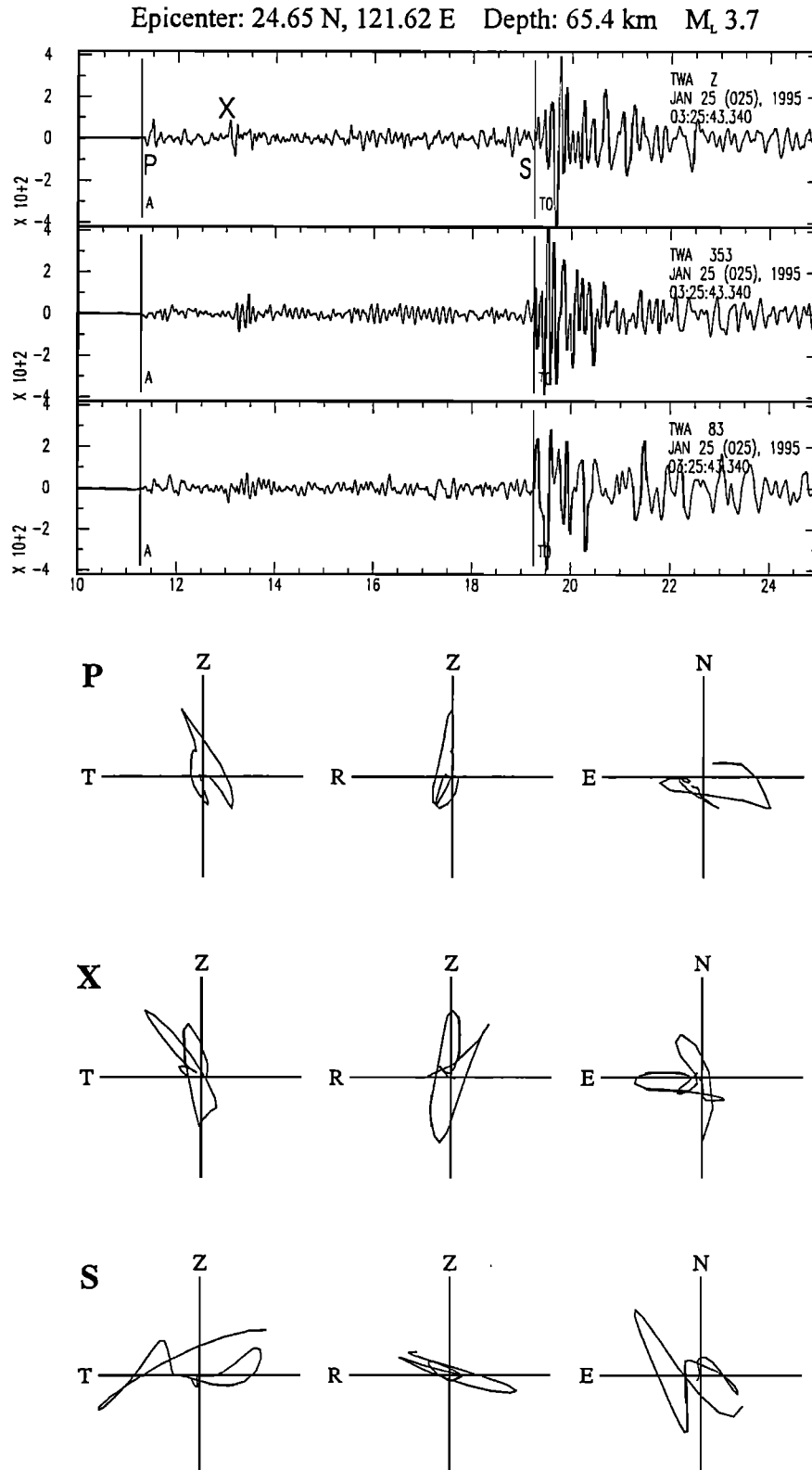
Epicenter: 24.65 N, 121.62 E   Depth: 65.4 km   M$_L$ 3.7

Figure 6a. (top) Seismograms (horizontal and vertical axes in second and digital count, respectively) and (bottom) associated particle motions showing a clear example of phase conversion. The converted phase (marked as "X") is 1.69 s after the *P* and 6.25 s before the *S*. Because the particle motion of the converted phase resembles that of *P* rather than *S*, we conclude that it is probably an *S* to *P* conversion at the top boundary of the subducted plate. The relative timing suggests that the boundary is located 17-20 km above the hypocenter.
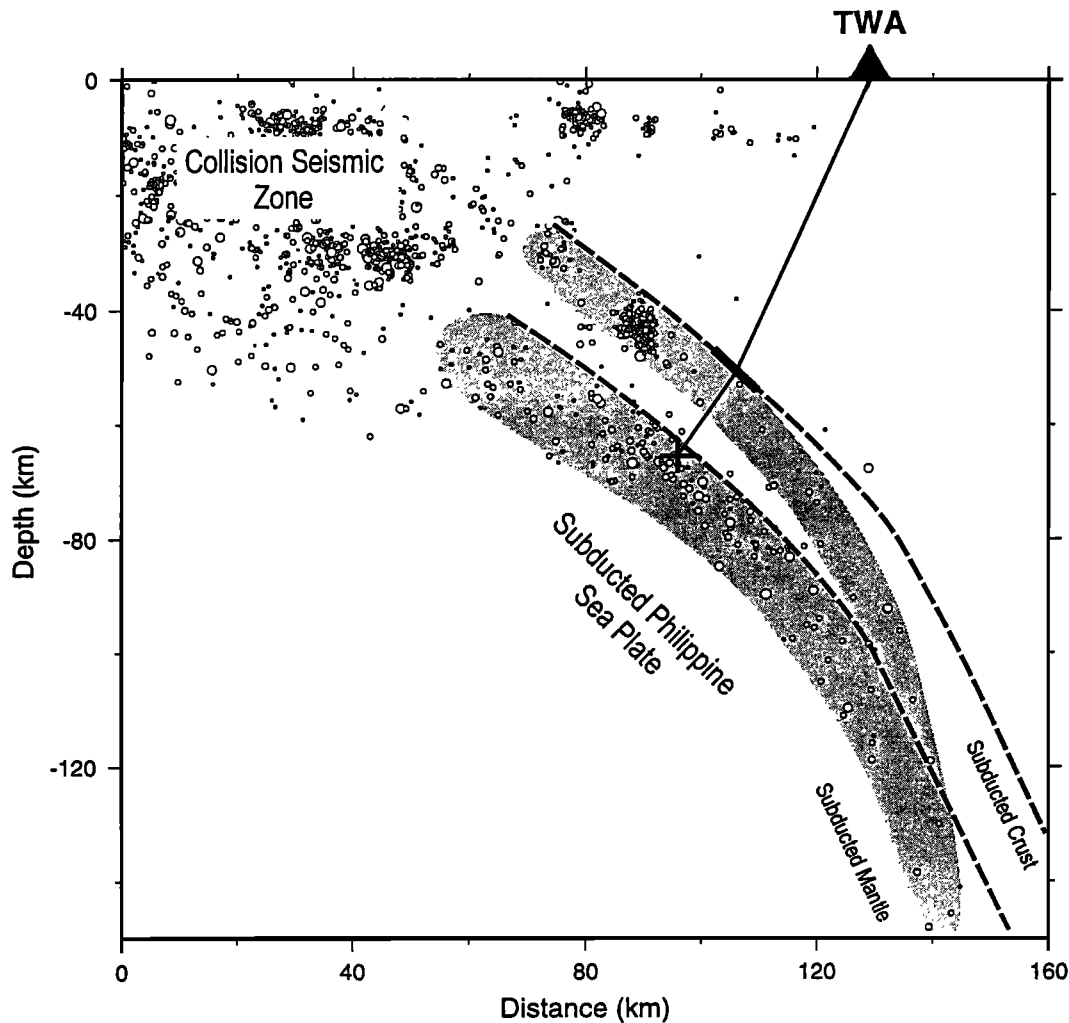
Figure 6b. A schematic diagram showing the configuration of a type II double seismic zone in NE Taiwan. Background seismicity is adapted from Plate 2a. Dashed lines mark the inferred upper boundaries of the subducted crust and mantle, whereas a thick solid line shows the portion confirmed by the converted phase (Figure 6a). The two layers of seismicity represent earthquakes occurring in the subducted upper crust and uppermost mantle, respectively. With increasing depth, the separation between the two layers decreases and earthquakes begin to migrate toward the interior of the subducted plate.

Chen, 1994, 1995; *Gorbatov et al.*, 1994], the Aleutian–Alaska arc [e.g., *Engdahl and Scholz*, 1977; *House and Jacob*, 1982; *Reyners and Coles*, 1982], the Mariana arc [e.g., *Samowitz and Forsyth*, 1981], the Tonga arc [e.g., *Kawakatsu*, 1985], and the New Britain region [e.g., *McGuire and Wiens*, 1995].

A classic double seismic zone is characterized by an upper layer of seismicity with downdip compressional focal mechanisms and a lower layer in downdip extension. The two layers initiate at a depth of approximately 70 km with a distance of 35–40 km in between. The separation decreases with increasing depth and the two layers merge into a single layer at depths of approximately 200 km.

To prevent further confusion between the double seismic zone mentioned above and the one we observed beneath NE Taiwan, we propose to term the two as "type I" and "type II," respectively. The geometry of a type II double seismic zone differs from that of a type I in several aspects, as summarized in Table 2. First, the lower layer of seismicity initiates at a

much shallower depth, around 20–40 instead of 70 km. Second, the separation between the two layers is at most 15±5 km, which is approximately half of that observed for a type I double seismic zone. Furthermore, the merge of the two layers takes place at a much shallower depth (≤150 km).

Notice that a type II double seismic zone is hard to identify because the smaller separation between the two layers requires a higher resolution in locating earthquake hypocenters, a condition not easily met by most local networks on island arcs. Fortunately, the situation has improved significantly over the past decade, mainly due to the rapid advance in the technical aspect of seismological observation and a better understanding of velocity structures in subduction zones. It is rather encouraging to note that NE Taiwan is not the only place on Earth where a type II double seismic zone is observed. Similar examples were recently documented for the subduction zones in New Zealand near the southernmost North Island [e.g., *Eberhart-Phillips and Reyners*, 1997; *Reyners et al.*, 1997], in Cascadia just north of the Mendocino

Table 2. Geometric Differences Between Type I and Type II Double Seismic Zones

Features	Type I	Type II
Commence of the lower layer, km	~70	20–40
Separation between the two layers, km	35–40	15±5
Merging depth of the two layers, km	~200	<150

triple junction [e.g., *Smith and Knapp*, 1993; *Wang and Rogers*, 1994], and in the Cook Inlet area, Alaska [e.g., *Ratchkovsky et al.*, 1997].

4.2. Characteristic Tectonic Setting: Termini of Oblique Subduction and Lateral Compression

Figure 7 shows the overall tectonic settings and cross sections for the New Zealand, Cascadia, and Alaska regions where the type II double seismic zones were reported. Despite that NE Taiwan seems to differ from these regions in many aspects, it is rather interesting to find a common tectonic characteristic among them.

Beneath NE Taiwan, the double seismic zone is observed along the westernmost segment of the subducted plate, less than 50 km from the terminus along the 121.5°E meridian (Plate 1 and Figure 4). The Philippine Sea plate is moving along 310° at 7 cm yr^{-1} (Figure 1) [*Seno et al.*, 1993], resulting in a significant oblique subduction such that the westward component is approximately parallel to the strike of the slab [e.g., *Fitch*, 1972; *Shiono et al*, 1980; *Kao et al.*, 1998a]. This lateral compression is clearly shown by the consistent orientation of P axes in earthquake focal mechanisms (Figures 2 and 3) [*Kao and Chen*, 1991; *Kao et al.*, 1998a].

Similarly, the double seismic zone observed in New Zealand is located near the southernmost North Island where the subduction system is changing into a transform fault (Figure 7a). The relative motion between the Pacific plate and the Australian plate is highly oblique to the trench normal direction [e.g., *DeMets et al.*, 1994], a setting basically similar to that in the southernmost Ryukyu. *Reyners et al.* [1997] studied earthquake focal mechanisms occurring in the region and reported low-angle thrust events just above the upper seismic layer between 12 and 25 km. The majority of earthquakes within the lower seismic layer (8 out of 12) show mechanisms with P and T axes parallel to the strike and dip of the subducted slab, respectively. It is particularly true for the region south of Cook Strait, within 150 km of the subducted slab's terminus. This pattern is analogous to the observations in NE Taiwan (Plate 1 and Figure 3).

In the southernmost Cascadia subduction zone near the Mendocino triple junction, a double seismic zone is documented at depths as shallow as 15–20 km [e.g., *Smith and Knapp*, 1993; *Wang and Rogers*, 1994]. Despite that the detailed tectonic configuration of this region is very complicated and still under vigorous debate [e.g., *Schwartz*, 1995; *Smith and Knapp*, 1993; *Wang and Rogers*, 1994; *Wang et al.*, 1997; *Wilson*, 1989, 1993], the overall tectonic framework is well understood. There are three major components: an oblique subduction system between the Gorda plate and North America plate, an E–W Mendocino transform fault that separates

the Gorda plate from the Pacific plate, and the so-called "Gorda Deformation Zone" to the north of the Mendocino transform fault (Figure 7b). Plate kinematics and numerical modeling both indicate that the region is under strong N–S (lateral) compression, most likely due to the northward push of the Pacific plate [e.g., *Wang et al.*, 1997; *Wilson*, 1989, 1993]. Earthquake focal mechanisms show that most events which occurred in the double seismic zone have P axes in N–S direction parallel to the strike of subducted slab (lateral compression), whereas events farther to the east are in downdip extension (slab pull) [e.g., *Schwartz*, 1995; *Smith and Knapp*, 1993].

In Alaska near the Cook Inlet area (Figure 7c), a type II double seismic zone is delineated between 50 and 100 km [e.g., *Ratchkovsky et al.*, 1997]. This region is practically the eastern end of the Alaska–Aleutian arc system. Global plate motion models predict an oblique subduction setting with a 30°–40° difference between the trench normal and the relative plate convergence directions [e.g., *DeMets et al.*, 1994; *Larson et al*, 1997]. Recent stress inversion using earthquake focal mechanisms indicates that the predominating stress field within the subducted slab is a combination of downdip extension and along-arc (i.e., lateral) compression [e.g., *Lu et al.*, 1997].

In conclusion, all regions where type II double seismic zones are found seem to share a common tectonic setting, namely, oblique subduction with significant lateral compression between the subducted plate and the adjacent lithosphere. Furthermore, all of them are within a short distance from the termini of the subducted slabs where the lateral compression is expected to be the greatest.

4.3. Seismogenic Origin

As demonstrated that a type II double seismic zone is unique in its geometry and tectonic characteristic, does it mean that the seismogenic origin of a type II double seismic zone is fundamentally different from that of a type I? Given the knowledge we have, how much can we address this issue?

Generally speaking, the occurrence of earthquakes requires two conditions. The first is the presence of sufficient deviatoric stress that generates the shear deformation and the second is the adequate mechanism(s) that can store and release the strain in a seismogenic way. The occurrence of a double seismic zone is getting more complicated because we need to simultaneously explain seismogenesis along both layers. As far as the source of stress is concerned, proposed interpretations include unbending of the subducted plate [e.g., *Engdahl and Scholz*, 1977; *Kawakatsu*, 1986], thermoelastic stresses [e.g., *Fujita and Kanamori*, 1981; *Hamaguchi et al.*, 1983; *House and Jacob*, 1982], and sagging of the subducted slab [e.g., *Sleep*, 1979].

On the other hand, possible seismogenic mechanisms for a double seismic zone were addressed much less in the literature. At shallow depths, brittle failure is the predominant seismogenic mechanism for earthquakes [e.g., *Scholz*, 1990]. At intermediate depths, brittle failure due to increasing pore pressure, which probably resulted from dehydration of hydrate minerals in the crust, is believed to be responsible for most seismogenesis [e.g., *Raleigh and Paterson*, 1965; *Meade and Jeanloz*, 1989]. An alternative is to attribute to the metastable phase transition from basalt to eclogite [e.g., *Fukao et al.*, 1983; *Pennington*, 1983; *Ringwood and Green*, 1966].
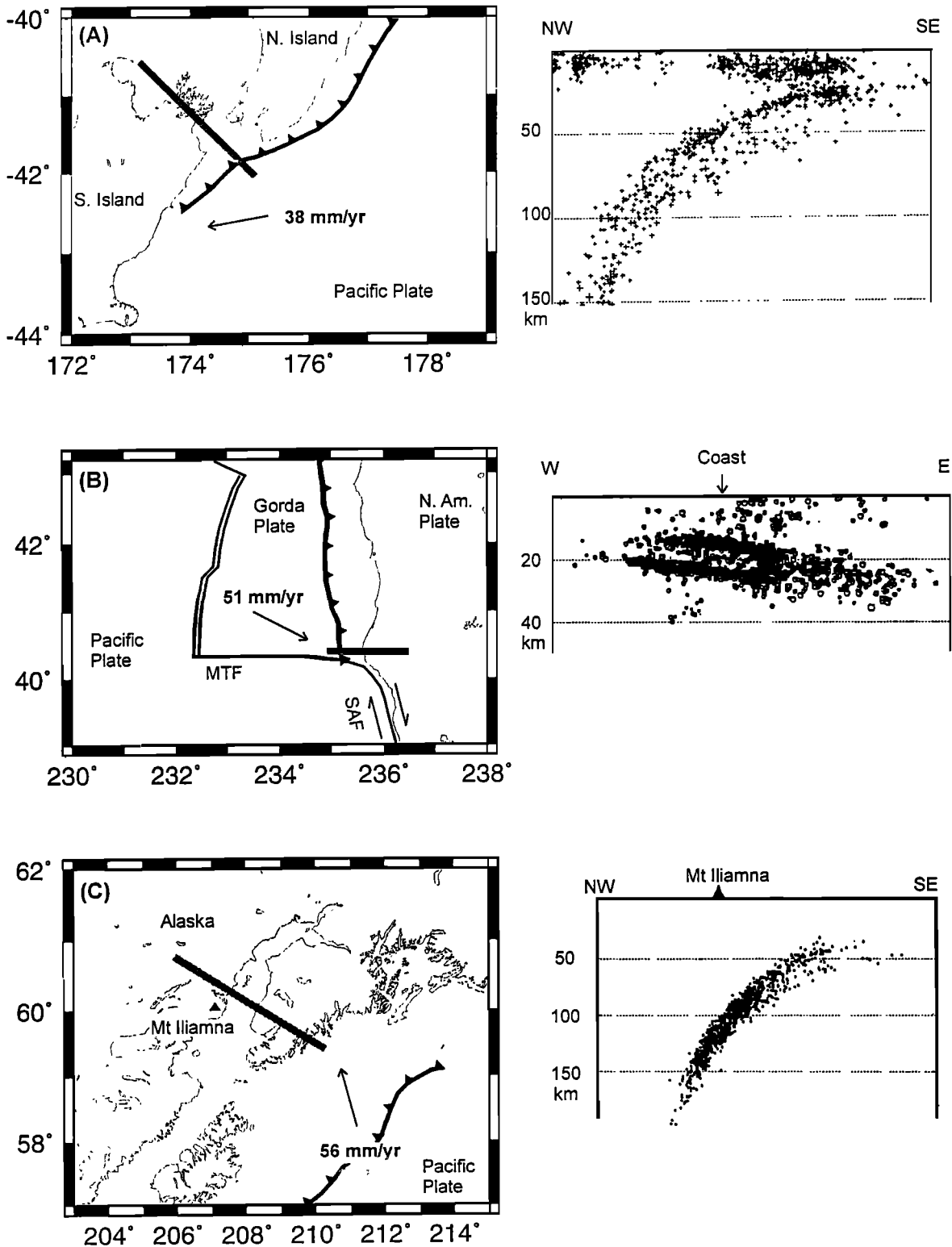
Figure 7. (left) Maps and (right) cross sections showing tectonic settings and distributions of seismicity for regions where type II double seismic zones were documented. Arrows show the directions of relative plate motions. Thick gray lines mark the locations of cross sections. (a) New Zealand near the southernmost North Island. (b) Cascadia just north of the Mendocino triple junction where the Mendocino Transform Fault (MTF), San Andreas Fault (SAF), and Cascadia subduction zone meet. (c) Cook Inlet area, Alaska. Notice that all regions are located within a short distance from the termini of subducted slabs and share a characteristic tectonic setting of oblique subduction with significant lateral compression between the subducted plate and the adjacent lithosphere.

Both arguments seem to apply only to the upper layer of a double seismic zone where both hydrate minerals and basalt are available. The occurrence of earthquakes in the lower layer, however, remains a puzzle.

Kao and Liu [1995] study seismic patterns and the temperature-pressure conditions associated with a classic double seismic zone. They propose the metastable phase transition from Al-rich enstatite (pyroxene) to Al-poor enstatite plus garnet to be a possible seismogenic mechanism for earthquakes occurring in the lower layer and part of the upper layer (> ~110 km). Alternatively, *Seno and Yamanaka* [1996] report a correlation between the existence of double seismic zones and deep outer rise compressional earthquakes. His interpretation calls for dehydration of solidified magma entrapped within the plate when it passed the head of a superplume somewhere on its way from mid-ocean ridges to subduction zones. Unfortunately, both models are inadequate to explain a type II double seismic zone because the observed lower layer begins at a depth where the temperature and pressure conditions are not ready for metastable phase transition of Al-rich enstatite, and there are no deeper compressional earthquakes in the corresponding outer-rise regions.

We propose that the compressive stress between the end of a subducted plate and the adjacent lithosphere (i.e., the lateral component of the oblique subduction) to be the source of stress responsible for type II double seismic zones. This stress regime, together with the downdip extension from slab pulling force, can explain the consistent patterns of lateral compression and downdip extension shown by most focal mechanisms found in type II double seismic zones.

From our observations alone, it is somewhat difficult to determine the corresponding seismogenic mechanism(s). Nonetheless, because the 15±5 km separation between the two layers is comparable to the thickness of the crust, it is possible to regard the observed upper seismic layer as seismicity occurred in the upper crust of a subducted plate and/or along the plate interface, whereas the lower layer is associated with events in the uppermost mantle (Figure 6b). If so, then interpretation for the seismogenesis of type II double seismic zones becomes rather straightforward. The scenario is analogous to that observed in a continental setting [e.g., *Chen and Molnar*, 1983] and basically reflects the variation of rheological strength of subducted materials, with a ductile (aseismic) lower crust sandwiched by a strong upper crust and a strong uppermost mantle (both seismic). As the slab penetrates to greater depth and reaches the appropriate temperature/pressure conditions for metastable phase transitions, the two layers merge into one seismic zone and earthquakes begin to migrate into the subducted mantle [*Kao and Liu*, 1995]. In fact, *Wang et al.* [1997] specifically calculates the differential stress distribution for the southernmost Cascadia subduction zone near the Mendocino triple junction and confirms that the observed type II double seismic zone is physically compatible with such a conclusion.

It is noted that the separation (15±5 km) between the two layers of the type II double seismic zone observed beneath NE Taiwan is slightly larger than the thickness of a normal oceanic crust (~10 km). We attribute it to the possible crustal thickening, which in turn, is due to the collision between the Philippine Sea and Eurasia plates in the region. A recent earthquake study using local broadband data confirms that there is significant thrust deformation within the Philippine Sea plate offshore east of Taiwan [*Kao et al.*, 1998b]. In ad-

dition, because the Coastal Range, which is part of the former Luzon arc, is located directly updip of the observed type II double seismic zone, the thickened crust might also correspond to the subducted arc materials.

4.4. A Testable Case: the Indo-Burma Subduction Zone

If our proposed model is correct, a type II double seismic zone should be observed in a region if it satisfies three conditions: significant oblique subduction, near the terminus of a subduction zone, and existence of considerable lateral compression between the subducted slab and the adjacent lithosphere. In addition to the four cases shown in Plate 2 and Figures 5 and 7, here we propose that the subduction system beneath the Indo-Burma ranges to be another place where a type II double seismic zone might exist.

The N–S striking Indo-Burma subduction system is bounded by the Himalaya Collision Zone to the north. Along it, the Indian plate obliquely subducts beneath the Eurasia [e.g., *Curray et al.*, 1979]. *Chen and Molnar* [1990] reported that the majority of large and moderate-sized earthquakes in the region shows a consistent pattern of N–S (lateral) compression, despite that the N–S trending Indo-Burma ranges seems to imply an E–W compression. They interpret that the deformation in the Indo-Burma ranges is decoupled from that in the underlying Indian plate such that the observed pattern of lateral compression reflects the state of strain within the subducted slab. *Ni et al.* [1989] determined the geometry of the subducted plate from 184 hypocenters reported by the International Seismological Centre (ISC) and concluded that lateral compressive earthquakes indeed occurred beneath the inferred plate interface.

Unfortunately, distribution of earthquakes reported in the ISC bulletins is too scattered to well define the expected two-layered structure. Furthermore, to our best knowledge, no detailed study of 3-D tomography and/or microearthquake relocation has been done for the region at the same resolution level as for those presented in Plate 2 and Figures 5 and 7. Hence, the existence of a type II double seismic zone cannot be confirmed at this moment. Nonetheless, our model can be tested should comparable studies become available in the future.

4.5. Dip Increase of WBZ and Regional Collision

In addition to the lateral compression transmitted within the subducted slab, the unique tectonic setting might also affect the geometry of the subducted plate as well. From our results, the dip of the subducted Philippine Sea plate increases significantly with depth, particularly for depths greater than ~90 km. This is evident both from the tomographic images and the distribution of earthquake hypocenters (Plate 2 and Figure 5).

The gravitational instability is certainly one of the most straightforward interpretations for the geometric variation of a subducted slab. On the basis of our previous discussion, there are major phase transitions at this depth range that can contribute to the dip increase (e.g., dehydration, basalt/gabbro to eclogite transition, and Al-rich enstatite to Al-poor enstatite plus garnet). In addition, the seismogenic model of *Kao and Liu* [1995] suggests that intermediate-depth earthquakes would gradually migrate toward the interior of the subducted plate, causing an apparent dip increase of WBZ that is slightly larger than that of the slab itself (Figure 6b).

Kao et al. [1998a] studied local seismicity and earthquake focal mechanisms for the southernmost Ryukyu–NE Taiwan region. They concluded that the interplate thrust zone between the Philippine Sea plate and Eurasia plate is greatly distorted as the Ryukyu trench approaches Taiwan and that the interface gradually migrates northward from ~23.5°N in the southernmost Ryukyu to ~24°N near the coastline of Taiwan. Since their results show no significant distortion in the geometry of subducted plate at intermediate depths, such a configuration implies an increase in the dip of WBZ. This scenario is in a way similar to the sea anchoring effect observed in Mariana except that here the arcward migration of plate interface is driven by the push of the regional collision instead of the overriding plate moving away from the trench [e.g., *Scholz and Campos*, 1995; *Uyeda and Kanamori*, 1979; *Wu*, 1978a]. Thus we propose that the regional collision is another, and probably significant, contributor to the steepening of the subducted Philippine Sea plate.

Notice the collision is most effective within the lithosphere, hence it is expected to find the biggest dip increase immediately below the bottom of the overriding plate (presumably at ~90–100 km). This is consistent with our observation in NE Taiwan (Plate 2 and Figure 5), New Zealand, and Alaska (Figure 7). As for the subduction zone in Cascadia near Mendocino triple junction, the system does not seem to reach the scale of regional collision. Also, the subducted slab does not extend to the intermediate depth. Therefore we expect no obvious geometric change to be found there.

5. Conclusion

The tectonic setting of northeast Taiwan is complicated by the simultaneous presence of oblique subduction, region collision, and back arc opening. Detailed structures of the subducted Philippine Sea plate beneath the region are mapped by seismic tomography using high-quality digital data recorded by the Taiwan Seismic Network. We further supplement the inversion results with earthquake source parameters determined from inversion of teleseismic P and SH waveforms. This step is critical to define the position of the plate interface and hence avoid the possibility of mistaking the interplate thrust zone or structures in the overriding plate as the WBZ. The most interesting feature is that earthquakes within the subducted Philippine Sea plate tend to occur along a two-layered structure (a double seismic zone). The location of the upper layer is immediately below the interplate thrust zone and extends down to 70–80 km at a dip of 40°–50°. Below approximately 100 km, the dip increases dramatically to 70°–80°. The lower layer commences at 45–50 km and maintains approximately parallel to the upper layer with a separation of 15±5 km in between. Below ~70–80 km, the separation decreases and they seem to gradually merge into one WBZ.

To avoid further confusion, we propose to term the classic double seismic zones observed beneath Japan and Kuril as "type I" and that we observed as "type II," respectively. A global survey of major subduction zones indicates that type II double seismic zones were also documented in three other regions: New Zealand near the southernmost North Island, Cascadia just north of the Mendocino triple junction, and the Cook Inlet area of Alaska. All of them are located within a short distance from the termini of subducted slabs and share a characteristic tectonic setting of oblique subduction with significant lateral compression between the subducted plate and the adjacent lithosphere.

We interpret the seismogenesis of type II double seismic zones as reflecting the lateral compressive and downdip extensional stresses originating from oblique subduction and slab pulling force, respectively. The upper seismic layer represents seismicity occurring in the upper crust of the subducted plate and/or along the plate interface, whereas the lower layer is associated with events in the uppermost mantle. The scenario is analogous to that observed in a continental setting and basically reflects the variation of rheological strength of subducted materials, with a ductile (aseismic) lower crust sandwiched by a strong upper crust and a strong uppermost mantle (both seismic).

References

Chen, W.-P., and P. Molnar, Focal depths of intracontinental earthquakes and their implications for the thermal and mechanical properties of the lithosphere, *J. Geophys. Res.*, *88*, 4183–4214, 1983.

Chen, W.-P., and P. Molnar, Source parameters of earthquakes and intraplate deformation beneath the Shillong plateau and the northern Indoburman ranges, *J. Geophys. Res*, *95*, 12,527–12,552, 1990.

Curray, J.R., D.G. Moore, L.A. Lawver, F.J. Emmel, R.W. Raitt, M. Henry, and R. Kieckhefer, Tectonics of the Andaman Sea and Burma, in *Geological and Geophysical Investigations of Continental Margins*, edited by J.S. Watkins, L. Montadert, and P. Dickerson, *AAPG Mem*, *29*, 189–198, 1979.

DeMets, C., R. Gordon, D. Argus, and S. Stein, Effect of recent revisions to the geomagnetic reversal time scale on estimates of current plate motions, *Geophys. Res. Lett.*, *21*, 2191–2194, 1994.

Dziewonski, A.M., J.E. Franzen, and J.H. Woodhouse, Centroid-moment tensor solutions for January–March, 1985, *Phys. Earth Planet. Inter.*, *40*, 249–258, 1985.

Dziewonski, A.M., G. Ekström, J.E. Franzen, and J.H. Woodhouse, Centroid-moment tensor solutions for January– March, 1986, *Phys. Earth Planet. Inter.*, *45*, 1–10, 1987a.

Dziewonski, A.M., G. Ekström, J.E. Franzen, and J.H. Woodhouse, Global seismicity of 1978: Centroid-moment tensor solutions for 512 earthquakes, *Phys. Earth Planet. Inter.*, *46*, 316–342, 1987b.

Dziewonski, A.M., G. Ekström, J.E. Franzen, and J.H. Woodhouse, Global seismicity of 1981: Centroid-moment tensor solutions for 542 earthquakes, *Phys. Earth Planet. Inter.*, *50*, 155–182, 1988.

Eberhart-Phillips, D., and M. Reyners, Continental subduction and three-dimensional crustal structure: The norhern South Island, New Zealand, *J. Geophys. Res.*, *102*, 11,843–11,861, 1997.

Engdahl, E.R., Seismicity and plate subduction in the central Aleutians, in *Island Arcs, Deep Sea Trenches, and Back-Arc Basins, Maurice Ewing Ser.*, vol. 1, edited by M. Talwani and W.C. Pitman III, pp. 259–271, AGU, Washington, D. C., 1977.

Engdahl, E.R., and C.H. Scholz, A double Benioff zone beneath the central Aleutians: An unbending of the lithosphere, *Geophys. Res. Lett.*, *4*, 473–476, 1977.

Evans, J.R., D. Eberhart-Phillips, and C.H. Thurber, User's manual for SIMULPS12 for imaging Vp and Vp/Vs: A derivative of the "Thurber" tomographic inversion SIMUL3 for local earthquakes and explosions, *U.S. Geol. Surv. Open File Rep.*, *94-431*, 1994.

Fitch, T.J., Plate convergence, transcurrent faults, and internal deformation adjacent to southeast Asia and the western Pacific, *J. Geophys. Res.*, *77*, 4432–4460, 1972.

Frohlich, C., S. Billington, E.R. Engdahl, and A. Malahoff, Detection and location of earthquakes in the central Aleutian subduction zone using island and ocean bottom seismograph stations, *J. Geophys. Res.*, *87*, 6853–6864, 1982.

Fujita, K., and H. Kanamori, Double seismic zones and stresses of intermediate depth earthquakes, *Geophys. J. R. Astron. Soc.*, *66*, 131–156, 1981.

Fukao, Y., S. Hori, and M. Ukawa, A seismological constraint on the depth of basalt-eclogite transition in a subducting oceanic crust, *Nature*, *303*, 413–415, 1983.

Gorbatov, A., G. Suárez, V. Kostoglodov, and E. Gordeev, A double-planed seismic zone in Kamchatka from local and teleseismic data, *Geophys. Res. Lett.*, *21*, 1675–1678, 1994.

Hamaguchi, H., K. Goto, and Z. Suzuki, Double-planed structure of intermediate-depth seismic zone and thermal stress in the descending plate, *J. Phys. Earth*, *31*, 329–347, 1983.

Hasegawa, A., N. Umino, and A. Takagi, Double-planed deep seismic zone and upper-mantle structure in the northeastern Japan arc, *Geophys. J. R. Astron. Soc.*, *54*, 281–296, 1978.

Hauksson, E., Structure of the Benioff zone beneath the Shumagin Islands, Alaska: Relocation of local earthquakes using three-dimensional ray tracing, *J. Geophys. Res.*, *90*, 635–649, 1985.

House, L.S., and K.H. Jacob, Thermal stresses in subducting lithosphere can explain double seismic zones, *Nature*, *295*, 587–589, 1982.

James, D.E., and J.A. Snoke, Structure and tectonics in the region of flat subduction beneath central Peru: Crust and uppermost mantle, *J. Geophys. Res.*, *99*, 6899–6912, 1994.

Kao, H., and W.-P. Chen, Earthquakes along the Ryukyu–Kyushu arc: Strain segmentation, lateral compression, and the thermomechanical state of the plate interface, *J. Geophys. Res.*, *96*, 21,443–21,485, 1991.

Kao, H., and W.-P. Chen, The double seismic zone in Kuril-Kamchatka: The tale of two overlapping single seismic zones, *J. Geophys. Res.*, *99*, 6913–6930, 1994.

Kao, H., and W.-P. Chen, Transition from interplate slip to double seismic zone along the Kuril–Kamchatka arc, *J. Geophys. Res.*, *100*, 9881–9903, 1995.

Kao, H., and L. Liu, A hypothesis for the seismogenesis of double seismic zone, *Geophys. J. Int.*, *123*, 71–84, 1995.

Kao, H., S.J. Shen, and K.-F. Ma, Transition from oblique subduction to collision: Earthquakes in the southernmost Ryukyu arc–Taiwan region, *J. Geophys. Res.*, *103*, 7211–7229, 1998a.

Kao, H., P.-R. Jian, K.-F. Ma, B.-S. Huang, and C.-C. Liu, Moment-tensor inversion for offshore earthquakes east of Taiwan and their implications to regional collision, *Geophys. Res. Lett.*, *25*, 3619–3622, 1998b.

Kawakatsu, H., Double seismic zone in Tonga, *Nature*, *316*, 53–55, 1985.

Kawakatsu, H., Double seismic zones: Kinematics, *J. Geophys. Res.*, *91*, 4811–4825, 1986.

Kawakatsu, H., and T. Seno, Triple seismic zone and the regional variation of seismic along the northern Honshu arc, *J. Geophys. Res.*, *88*, 4215–4230, 1983.

Larson, K.M., J.T. Freymueller, and S. Philipsen, Global plate velocities from the Global Positioning System, *J. Geophys. Res.*, *102*, 9961–9981, 1997.

Lee, T.-Y., and L.A. Lawver, Cenozoic plate reconstruction of the South China Sea region, *Tectonophysics*, *235*, 149–180, 1994.

Liu, C.-C., The Ilan plain and the southwestward extending Okinawa trough, *J. Geol. Soc. China*, *38*, 229–242, 1995.

Lu, Z., M. Wyss, and H. Pulpan, Details of stress directions in the Alaska subduction zone from fault plane solutions, *J. Geophys. Res.*, *102*, 5385–5402, 1997.

Matsuzawa, T., N. Umino, A. Hasegawa, and A. Takagi, Upper mantle velocity structure estimated from PS-converted wave beneath the north-eastern Japan arc, *Geophys. J. R. Astron. Soc.*, *86*, 767–787, 1986.

McGuire, J.J., and D.A. Wiens, A double seismic zone in New Britain and the morphology of the Solomon Plate at intermediate depths, *Geophys. Res. Lett.*, *22*, 1965–1968, 1995.

McLaren, J.P., and C. Frohlich, Model calculations of regional network locations for earthquakes in subduction zones, *Bull. Seismol. Soc. Am.*, *75*, 397–413, 1985.

Meade, C., and R. Jeanloz, Acoustic emissions and shear instabilities during phase transformations in Si and Ge at ultrahigh pressures, *Nature*, *339*, 616–618, 1989.

Menke, W., *Geophysical Data Analysis. Discrete Inverse Theory*, 289 pp., Academic Press, San Diego, Calif., 1989.

Nábelek, J.L., Determination of earthquake source parameters from inversion of body waves, Ph.D. thesis, Mass. Inst. of Technol., Cambridge, 1984.

Ni, J.F., M. Guzman-Speziale, M. Bevis, W.E. Holt, T.C. Wallace, and W.R. Seager, Accretionary tectonics of Burma and the three-dimensional geometry of the Burma subduction zone, *Geology*, *17*, 68–71, 1989.

Ouchi, T., and H. Kawakami, Microseismicity in the middle Okinawa trough, *J. Geophys. Res.*, *94*, 10,601–10,608, 1989.

Pennington, W.D., Role of shallow phase changes in the subduction of oceanic crust, *Science*, *220*, 1045–1047, 1983.

Pezzopane, S.K., and S.G. Wesnousky, Large earthquakes and crustal deformation near Taiwan, *J. Geophys. Res.*, *94*, 7250–7264, 1989.

Raleigh, C.B., and M.S. Paterson, Experimental deformation of serpentinite and its tectonic implications, *J. Geophys. Res.*, *70*, 3965–3985, 1965.

Ratchkovsky, N.A., J. Pujol, and N.N. Biswas, Relocation of earthquakes in the Cook Inlet area, south Central Alaska using the joint hypocenter determination method, *Bull. Seismol. Soc. Am.*, *87*, 620–636, 1997.

Reyners, M., and K.S. Coles, Fine structure of the dipping seismic zone and subduction mechanics in the Shumagin Islands, Alaska, *J. Geophys. Res.*, *87*, 356–366, 1982.

Reyners, M., R. Robinson, and P. McGinty, Plate coupling in the northern South Island and southernmost North Island, New Zealand, as illuminated by earthquake focal mechanisms, *J. Geophys. Res.*, *102*, 15,197–15,210, 1997.

Ringwood, A.E., and D.H. Green, An experimental investigation of the gabbro-eclogite transformation and some geophysical implications, *Tectonophysics*, *3*, 383–427, 1966.

Samowitz, I.R., and D.W. Forsyth, Double seismic zone beneath the Mariana island arc, *J. Geophys. Res.*, *86*, 7013–7021, 1981.

Sato, T., Calculation of travel time and the partial derivatives for spherically-layered medium, *J. Seismol. Soc. Jpn.*, *31*, 340–342, 1978.

Sato, T., S. Koresawa, Y. Shiozu, F. Kusano, S. Uechi, O. Nagaoka, and J. Kasahara, Microseismicity of back-arc rifting in the middle Okinawa Trough, *Geophys. Res. Lett.*, *21*, 13–16, 1994.

Scholz, C.H., *The Mechanics of Earthquakes and Faulting*, 439 pp., Cambridge Univ. Press, New York, 1990.

Scholz, C.H., and J. Campos, On the mechanism of seismic decoupling and back arc spreading at subduction zones, *J. Geophys. Res.*, *100*, 22,103–22,115, 1995.

Schwartz, S.Y., Source parameters of aftershocks of the 1991 Costa Rica and 1992 Cape Mendocino, California, earthquakes from inversion of local amplitude ratios and broadband waveforms, *Bull. Seismol. Soc. Am.*, *85*, 1560–1575, 1995.

Seno, T., and G. Kroeger, A reexamination of earthquakes previously thought to have occurred within the slab between the trench axis and double seismic zone, northern Honshu arc, *J. Phys. Earth*, *31*, 195–216, 1983.

Seno, T., and Y. Yamanaka, Double seismic zones, compressional deep trench-outer rise events, and superplumes, in *Subduction Top to Bottom*, *Geophys. Monogr. Ser.*, vol. 96, edited by G.E. Bebout, D.W. Scholl, S.H. Kirby, and J.P. Platt, pp. 347–355, AGU, Washington, D. C., 1996.

Seno, T., S. Stein, and A.E. Gripp, A model for the motion of the Philippine Sea Plate consistent with NUVEL-1 and geological data, *J. Geophys. Res.*, *98*, 17,941–17,948, 1993.

Shin, T.-C., The calculation of local magnitude from the simulated Wood-Anderson seismograms of the short-period seismograms in the Taiwan area, *Terr. Atmos. Oceanic Sci.*, *4*, 155–170, 1993.

Shiono, K., T. Mikumo, and Y. Ishikawa, Tectonics of the Kyushu-Ryukyu Arc as evidenced from seismicity and focal mechanism of shallow to intermediate-depth earthquakes, *J. Phys. Earth*, *28*, 17–43, 1980.

Sibuet, J.-C., et al., Back arc extension in the Okinawa trough, *J. Geophys. Res.*, *92*, 14,041–14,063, 1987.

Sleep, N.H., The double seismic zone in downgoing slabs and the viscosity of the mesosphere, *J. Geophys. Res.*, *84*, 4565–4571, 1979.

Smith, S.W., and J.S. Knapp, Seismicity of the Gorda plate, structure of the continental margin, and an eastward jump of the Mendocino triple junction, *J. Geophys. Res.*, *98*, 8153–8171, 1993.

Spence, W., Slab pull and the seismotectonics of subducting lithosphere, *Rev. Geophys.*, *25*, 55–69, 1987.

Teng, L.S., Geotectonic evolution of late Cenozoic arc–continent collision, *Tectonophysics*, *183*, 57–76, 1990.

Thurber, C.H., Earthquake locations and three-dimension crustal structure in the Coyote Lake area, central California, *J. Geophys. Res.*, *88*, 8226–8236, 1983.

Thurber, C.H., Local earthquake tomography: Velocities and V_p/V_s– Theory, in *Seismic Tomography: Theory and Practice*, edited by H.M. Iyer and K. Hirahara, pp. 563–583, Chapman and Hall, New York, 1993.

Tsai, C.-S., M.-D. Lin, and Y.-B. Tsai, Relocation of the 12 March 1966 earthquake sequence in Northeast Taiwan offshore, Rep. ASIES-CR8306, Inst. of Earth Sci., Acad. Sinica, Taipei, Taiwan, 1983.

Umino, N., and A. Hasegawa, On the two-layered structure of deep seismic plane in northeastern Japan arc (in Japanese), *J. Seismol. Soc. Jpn*, *28*, 125–139, 1975.

Uyeda, S., and H. Kanamori, Back-arc opening and the mode of subduction, *J. Geophys. Res.*, *84*, 1049–1061, 1979.

Veith, K., The relationship of island arc seismicity to plate tectonics, Ph.D. thesis, South. Methodist Univ., Dallas, Tex., 1974.

Wang, K., and G.C. Rogers, An explanation for the double seismic layers north of the Mendocino triple junction, *Geophys. Res. Lett.*, *21*, 121–124, 1994.

Wang, K., J. He, and E.E. Davis, Transform push, oblique subduction resistance, and intraplate stress of the Juan deFuca plate, *J. Geophys Res.*, *102*, 661–674, 1997.

Wilson, D.S., Deformation of the so-called Gorda plate, *J. Geophys. Res.*, *94*, 3065–3075, 1989.

Wilson, D.S., Confidence intervals for motion and deformation of the Juan de Fuca plate, *J. Geophys. Res.*, *98*, 16,053–16,071, 1993.

Wu, F.T., Benioff zones, absolute motion and interarc basin, *J. Phys. Earth*, *26, suppl.*, S39–S54, 1978a.

Wu, F.T., Recent tectonics of Taiwan, *J. Phys. Earth*, *26, suppl.*, S265–S299, 1978b.

Yeh, Y.-H., C.-H. Lin, and S.W. Roecker, A study of upper crustal structures beneath northeastern Taiwan: Possible evidence of the western extension of Okinawa trough, *Proc. Geol. Soc. China*, *32*, 139–156, 1989.

Zhao, D., A. Hasagawa, and S. Horiuchi, Tomographic imaging of *P* and *S* wave velocity structure beneath northeastern Japan, *J. Geophys. Res.*, *97*, 19,909–19,928, 1992.

Zhao, D., T. Matsuzawa, and A. Hasegawa, Morphology of the subducting slab boundary in the northeastern Japan arc, *Phys. Earth Planet. Inter.*, *102*, 89–104, 1997.

H. Kao and R.-J. Rau, Institute of Earth Sciences, Academia Sinica, P.O. Box 1-55 Nankang, Taipei, Taiwan 115, ROC (e-mail: kao@earth.sinica.edu.tw)